TEL AVIV UNIVERSITY

Plastic, Air, Alcohol And Cigars Through The Lens Of An IR Spectrometer

Alon Shaaltiel,[1] Oren Kereth,[1] and Georgi Gary Rozenman[1,2]

[1] *Raymond and Beverly Sackler School of Physics and Astronomy, Faculty of Exact Sciences, Tel Aviv University, Tel Aviv 69978, Israel*

[2] *School of Electrical Engineering, Iby and Aladar Fleischman Faculty of Engineering, Tel Aviv University, Tel Aviv 69978, Israel*

(Dated: January 5, 2022)

Using FTIR and ATR spectroscopy we study the characteristics of gases, liquids and solids. When a light beam passes through a sample, certain wavelengths are absorbed depending on the sample's properties, thus allowing us to analyze the sample based upon its IR spectrum. Polyester's refractive index is found from thin film interference, alcohol concentrations in drinks are calculated, the molecular constants of carbon-monoxide are found and the ratio of carbon-dioxide in exhaled air compared to fresh air worryingly shows a downward trend through the years. Lastly, chemical products in various cigars' smoke are identified and a comparison between the cigars based on the toxicity of their contents is made.

1. INTRODUCTION

In this experiment the Fourier Transform Infra Red spectrometer (FTIR) will be used extensively to extract the infra-red spectrum of various materials and compounds. The infra-red spectrum consists of the intensity of incoming light made out of a range of wavelengths transmitted through a sample. The sample absorbs some wavelengths thus yielding an IR spectrum of that particular sample.

A short historical overview is presented for the reader, for more information see References. In 1800 IR was recognized as a distinct region of the energy spectrum by Sir William Herschel, however the study of IR light with various materials started about 100 years later. In 1903, William W.Coblentz measured the IR spectra of hundreds of inorganic and organic compounds[1]. As a result of increasing interest in the field, the first prototypes of IR spectroscopy were built in the 1930s. In 1949 the astrophysicist Peter Fellgett used an interferometer to measure light from celestial bodies and produced the first Fourier transform infrared spectrum, however this method was still limited and took many hours to compute. In the late 1960s, commercial FTIR spectrometers appeared as microcomputers were able to do the Fourier transform, however they were large and expensive. Over time, technology reduced the costs and size, increased availability and enhanced the capabilities of FTIR spectroscopy systems[2].

1.1. Thin Film Interference

Upon contact with a beam of light, the internal reflections in a thin sample of material with a sufficiently high refractive index are not negligible.

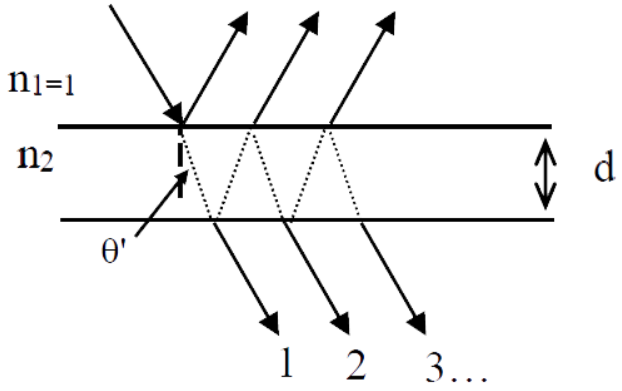

Figure 1. Reflected and transmitted light waves from a thin film

This experiment concerns only the transmitted beams; The treatment for reflected beams is quite similar.
In this experiment only the intensity of the beams is detected, to understand how coherent light beams with the same wavenumber, $\vec{k}$ (and frequency, ω) affect the detected intensity, an example of two beams is given. The electric fields, $\vec{E}$, of the two beams are

$$\vec{E}_i = E_i e^{i(\omega t - \vec{k}\cdot\vec{r}+\varphi_i)}\hat{\epsilon}_1;\ i = 1,2$$

where φ_i is the electromagnetic wave's phase shift and $\hat{\epsilon}_1$ is the polarization. The detectable wave is the super-position of both waves

$$\vec{E} = (E_1 + E_2 e^{i\Delta\varphi})e^{i(\omega t - \vec{k}\cdot\vec{r}+\varphi_1)}\hat{\epsilon}_1;\ \Delta\varphi = \varphi_2 - \varphi_1$$

An electromagnetic wave's intensity is proportional to $|\vec{E}|^2$ thus, the detected intensity is proportional to

$$|\vec{E}|^2 = E_1^2 + E_2^2 + \Re\{2E_1E_2e^{i\Delta\varphi}\}$$
$$\rightarrow I = I_1 + I_2 + 2\sqrt{I_1 I_2}cos(\Delta\varphi)$$

If $\Delta\varphi = 2n\pi;\ (n \in \mathbb{Z})$, I is at its maximum, this is called "constructive interference". If $\Delta\varphi = (2n+1)\pi;\ (n \in \mathbb{Z})$, I is at

its minimum, this is called "destructive interference". If $\Delta\varphi$ is changed linearly the detected intensity would result in a cosine\sine[3].
Now onto the transmitted beams, the phase between two consecutive transmitted beams and relative intensity are

$$\Delta\varphi = k(2n_2 dcos\theta) \tag{1}$$

where $k = \frac{2\pi}{\lambda}$ is the beam's wave number, λ is the beam's wave length, n_2 is the sample's refractive index, θ is the beam's angle inside the sample and d is the sample's thickness. $2n_2 dcos\theta$ is the optical path length (OPL) difference. Constructive interference occurs if OPL = $\frac{m}{k}$ and if OPL = $\frac{m+\frac{1}{2}}{k}$, destructive interference occurs, where $m \in \mathbb{Z}$. The difference in wavenumber (Δk) between two destructive peaks of intensity would be (Equation 1)

$$\Delta k = \frac{1}{2n_2 dcos(\theta)} \tag{2}$$

1.2. The Beer-Lambert Law

The Beer-Lambert Law describes how a monochromatic beam of light is absorbed in relation to substance concentration. The dependency is given by

$$\ln\left(\frac{P(\upsilon)}{P_0(\upsilon)}\right) = A = -a\upsilon_{\alpha\alpha'}Cx \tag{3}$$

where $P(\upsilon)$ is the light's intensity through the sample, $P_0(\upsilon)$ is the intensity with no sample, A is the absorbance, a is the molar attenuation coefficient, α and α' are quantum numbers, C is the concentration, and x is the optical path length of the beam, given by $n \cdot l$ where l is the distance the beam traveled and n is the material's refractive index. All else being equal, the absorbance and concentration are proportional to one another.
The Beer-Lambert Law does have its limitations, for starters, it is only valid for low concentrations, according to (LibreTexts, [4]) at higher concentrations "the individual particles of analyte no longer are independent of each other", this may change the material's absorptivity. On top of that, at high concentrations a solution's refractive index may change across concentrations [4].

1.3. CO Molecule IR Spectrum

The model used to describe CO molecules and other diatomic molecules pictures a molecule in which the individual atoms, held together by chemical bonds, are in vibratory motion along these bonds, while the molecule as a whole is rotating [5]. The energy states of this system correspond to a Hamiltonian with a potential

$$V(\boldsymbol{r}) = \frac{1}{2}k(r - r_0)^2 \tag{4}$$

and can be expressed as a combination of rotational and vibrational energies

$$E = E_{Rot} + E_{Vib} = hcw_e(v + \frac{1}{2}) + \frac{\hbar^2}{2I}J(J+1) \tag{5}$$

where h is Planck's constant, $\hbar$ is the reduced Planck's constant, c is the speed of light, w_e is the wave number corresponding to the frequency of vibrations, v is a quantum number corresponding to the vibrations, I is the molecule's moment of inertia and J is a quantum number corresponding to the angular momentum of the particle [6]. However, the current potential is not truly harmonic and only serves as an approximation, as effects such as the centrifugal force, Coriolis and Fermi [5] require the use of perturbation theory [7]. Using the perturbation theory, the energy states are now

$$\begin{aligned} &T = T_{Vib} + T_{Rot} = \\ &w_e(v+\frac{1}{2}) - w_e x_e(v+\frac{1}{2})^2 + \\ &B_v J(J+1) - D_v J^2(J+1)^2 \end{aligned} \tag{6}$$

where x_e, B_v and D_v are constants which take into account small perturbations and T is the energy states in wave number units ($T = \frac{E}{hc}$). At room temperature only the $v = 0$ state is occupied while the J states are all occupied. Therefore, using selection rules [6] only the transitions $v \to v'$ where $v' = 1,2,3$ and $J \to J'$ where $J' = J+1, J-1$ are of interest. Using equation 6 the allowed spectral lines are derived to be

$$\begin{aligned} &\Delta T = T(v', J') - T(0, J) = \\ &w_e v' - w_e x_e(v'^2) + (2B_e - \alpha(v'+1))m - \\ &\alpha v' m^2 - 4D_v m^3 \end{aligned} \tag{7}$$

where ΔT is the allowed spectral line, B_e, α are constants related to B_v which are the result of further corrections due to perturbation theory and m is either $J+1$ or $-(J-1)$ depending on the transition. In this experiment the transitions to $v' = 1$ and $v' = 2$ will be of interest, for which $\Delta T = 2141 cm^{-1}$ and $\Delta T = 4255 cm^{-1}$ respectively.

2. EXPERIMENTAL SYSTEM AND MEASUREMENTS

There are two main measuring instruments in this experiment- FTIR and ATR. Both use Michelson interferometers and perform a Fourier transform.

2.1. Michelson Interferometers

A Michelson interferometer consists of two perpendicularly plane mirrors, one of which can travel in a direction perpendicular to the plane. A semi reflecting film, the beamsplitter, bisects the planes of these two mirrors. The beamsplitter splits the beam into two, one beam transmitted through the beamsplitter and the other reflected from

it. Both beams then get reflected from the mirrors, returning to the beamsplitter where they recombine and interfere [8] (see Figure 2).

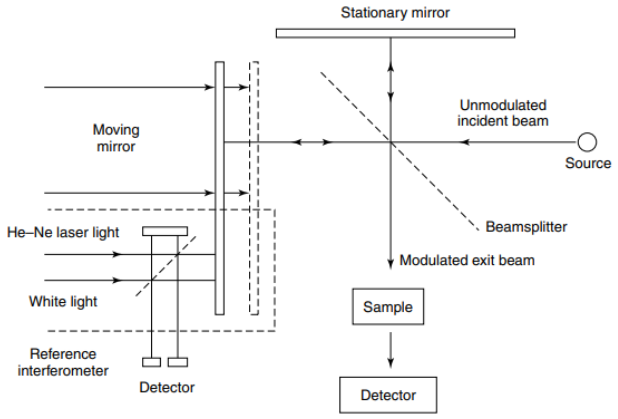

Figure 2. Schematic of a Michelson interferometer [8].

The beam which emerges from the interferometer at 90 degrees to the input beam is called the transmitted beam and is the beam detected by the detector as can be seen in Figure 2. The moving mirror produces an optical path difference between the two split beams. Plotting the signal produced by the detected beam as a function of the change of optical path length between the two beams yields an interferogram. By performing a Fourier transform on the interferogram the spectral distribution of the beam (i.e. the amplitude of each wave number the light is made of.) can be found.

2.2. FTIR

FTIR stands for Fourier Transform Infra-Red spectrometer. IR radiation is passed through a sample. Some infrared radiation is absorbed by the sample and some of it is passed through (transmitted). The resulting spectrum represents the molecular absorption and transmission [9]. FTIR (see Figure 3) utilizes Michelson interferometers, the interferogram and a Fourier transform to perform the analysis of the spectrum.

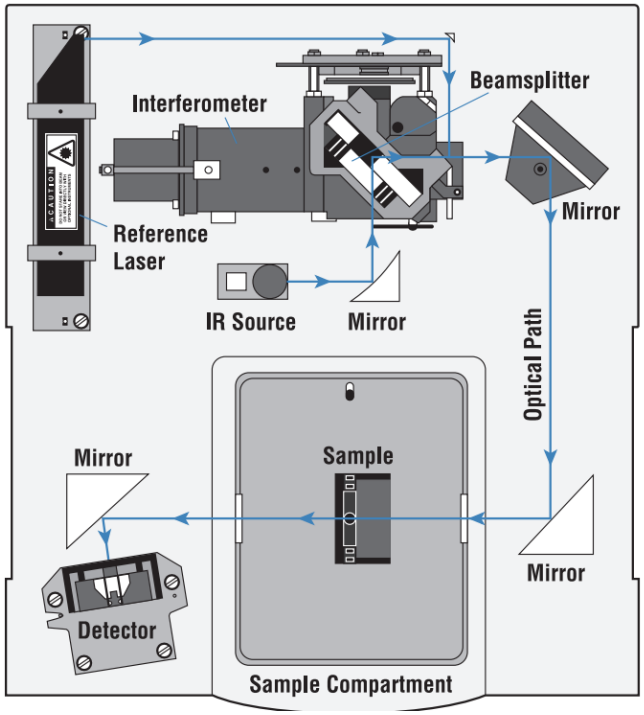

Figure 3. Layout of the FTIR spectrometer [9].

As can be seen in Figure 3, a black-body source emits IR radiation. The radiation then passes through an interferometer, where the 'spacial encoding' takes place [9]. A He-Ne laser is used as a reference for calibration of the moving mirror's position [8]. After going through the interferometer, an interferogram is created. The interferogram then passes through the sample, where specific wave numbers are absorbed according to the sample's characteristics and the rest are transmitted into the detector where the interferogram signal is measured. The data reaches the computer, which performs a Fourier transform yielding the infrared spectrum consisting of absorption lines corresponding to the sample.

2.3. ATR

ATR, which stands for *Attenuated Total Reflection*, measures the absorbance of a liquid or solid using IR spectroscopy. A crystal with a sufficiently high refractive index to achieve total internal reflection is surrounded by the material whose absorbance is of interest.

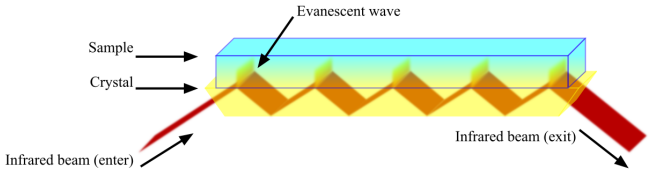

Figure 4. Layout of an ATR compartment [10]

An interferogram is projected into the crystal and evanescent waves, resulting from the total internal reflection, propagate through the sample. Evanescent waves penetrate the sample with an exponentially decreasing amplitude and intensity with distance. When no sample is inserted, and a vacuum surrounds the crystal, the energy evanescent waves carry is wholly returned $\langle \frac{dU_{Eva}}{dt} \rangle = 0$. However, if a sample is inserted into the ATR, and evanescent waves propagate through it, wave-lengths corresponding with the sample's normal modes are absorbed and the energy of the reflected beam decreases $\langle \frac{dU_{Eva}}{dt} \rangle < 0$. As described in the previous paragraph, the interferogram is detected and disassembled into the sample's infrared spectrum.

2.4. Transmission Through Thin Films of Polyester

In this part of the experiment the refractive index of a thin sample of polyester is extracted. Thin polyester samples with varying widths are placed in the sample area perpendicular to the beam's direction. An interferogram is projected through each sample. The resulting IR absorbance spectrum will be a summation of the material's (polyester's) absorbance spectrum and the sine wave showing absorption from thin film interference. To extract the frequency of destructive interference ($\frac{1}{\Delta k}$ in eq. 2) a sine wave is fitted to the region in the absorbance spectrum with the clearest sine wave, the fit's frequency is taken as the sample's frequency. Using equation 2, the extracted sine frequency, the measured width, and $\theta = \frac{\pi}{2}$, as the sample is perpendicular to the beam, a fit of the form

$$\begin{aligned} d &= a_0 + a_1 f_{fit} \\ f_{fit} &= \frac{1}{\Delta k};\ a_1 = 2n_2;\ a_0 \approx 0 \end{aligned} \tag{8}$$

was made. Some samples' widths were not measured and only had an interferogram projected through them. By fitting a sine to their IR spectra and inputting their fitted frequency into the calibrated relation in equation 8, their widths can be approximated.

2.5. Calibration Using Ethanol

In this part of the experiment the relationship between the concentration of a dissolved substance inside a solution to its total absorbance amplitude, which is assumed to be linear according to equation 3, was calibrated. The calibration was done using solutions of water and ethanol with varying known concentrations. The solution was put into a tank inside an ATR. Starting from a concentration of 96%, the ethanol was diluted by adding more water into the solution, thus changing the concentration of the ethanol according to

$$C_i V_i = C_f V_f \tag{9}$$

where C_i,V_i, C_f,V_f are the initial and final concentration of ethanol and volume of the solution respectively. The final measurement was at a 40% concentration of ethanol. For each concentration, C, the total absorbance of the solution in the range $1000-1120cm^{-1}$, F, was calculated. In this range lie the absorption peaks of ethanol [11] and therefore, according to equation 3 their intensity is proportional to the concentration of ethanol in the solution. A calibration graph of the form

$$C = a_0 + a_1 F \tag{10}$$

was then made. Using the calibration, the concentration of different solutions was found by calculating their total absorbance, F.

2.6. CO_2 and IR Spectrum of CO

Using a pump, exhaled and room air were each inserted into a chamber in the FTIR. For each of the two types of air the total absorbance in the range $2270-2400cm^{-1}$ was calculated. In this region there are two absorption peaks both corresponding to the concentration of CO_2 in the air. The ratio between the total absorbance of the exhaled air to the room air in that region, denoted by S is therefore equal to the corresponding ratio between CO_2 concentrations in each of them. S will then be compared to previously measured ratios. Afterwards, by pumping CO into to the same chamber in the FTIR, its IR spectrum was measured. According to equation 7 the spectrum contains absorption peaks that represent a transition in the angular momentum of the molecule, J to either $J+1$ or $J-1$ (see Figure 5).

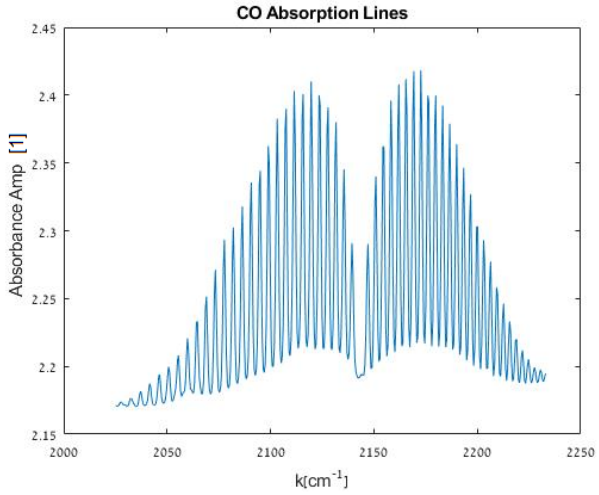

Figure 5. CO absorption lines in the region $2025-2233cm^{-1}$. Each peak represents a transition m of the angular momentum and the transition from $v=0$ to $v'=1$ which is centered at $2141cm^{-1}$ as can be seen and according to subsection 1.3.

Each of the peaks, m, were numbered according to its order relative to the center point at $2141 cm^{-1}$ (i.e. if m was the first to its left it was numbered as -1 and if it was the first to its right it was numbered as 1). Afterwards, a polynomial fit of 3^{rd} order was made between ΔT and m from equation 7

$$\Delta T = a_0 + a_1 m + a_2 m^2 + a_3 m^3 \tag{11}$$

The coefficients extracted from the fit will then be used to extract the coefficients in equation 7 according to the relations

$$\begin{aligned} \alpha &= -a_2 & D_v &= -\frac{a_3}{4} & w_e &= 2a_0 - \frac{4255}{2} \\ B_e &= \frac{a_1 - 2a_2}{2} & x_e &= \frac{a_0 - \frac{4255}{2}}{2a_0 - \frac{4255}{2}} \end{aligned} \tag{12}$$

where in order to find w_e and x_e the spectral line, $\Delta T = 4255 cm^{-1}$, of the transition $v = 0 \rightarrow v' = 2$ and $\Delta J = 0$ was used. The extracted values of the coefficients will then be compared to their corresponding theoretical values.

2.7. IR Spectra of Different Cigar Brands

In this part of the experiment gases in the smoke of various cigars are analyzed. An interferogram is projected through regular air. A pump smokes on a cigar and fills the sample area with smoke. An interferogram is projected through the smoke and the absorbance spectrum compared to regular air is created. Various toxic gases are identified. Each gas's total absorption (TA) was calculated using trapezoidal rule [12] and taken as a proxy to concentration. The TA of different substances cannot be compared; However, the TA of the same substance in different cigar brands can be directly compared. The comparison will look at the different substances and relative quantities and try to answer which is the most harmful.

3. RESULTS

3.1. Polyester Refractive Index Calculation

For each sample width the area with the clearest sine wave in the absorption spectrum was found and fitted to a sine wave.

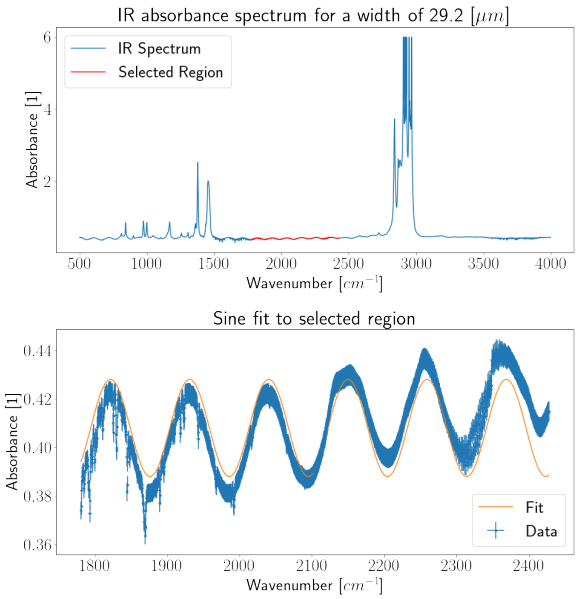

Figure 6. IR absorbance spectrum and sine fit to the selected region for a width of 29.2 [μm]

Fitting a linear function between the width and the frequency of the associated sine (eq. 8) yielded the following (See Figure 7)

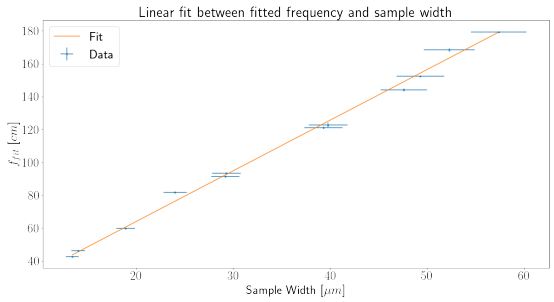

Figure 7. Linear fit between the fitted frequency, f_{fit}, and the sample width.

The fit's statistical measures are $P_{value} = 0.95$ and $\chi^2_{red} = 0.39$, both suggest a slight over-estimation of errors. The fit parameters of the linear fit can be seen in Table I

Fit Parameters of Width vs. Frequency		
Parameter	Value	Error (Relative Error)
$a_0[cm]$	2.4	1.5 (60%)
$a_1[1]$	3.080	0.060 (1.9%)

Table I. Fit parameters of the sample width vs. fitted frequency fit

Using equation 2, the extracted refractive index is

$$n = \frac{a_1}{2} = 1.540 \pm 0.030\ [1] \tag{13}$$

Using the calibrated correlation between sample width and sine frequency, the widths of three samples, whose widths were not measured but had an interferogram projected through them were approximated and can be seen in table II.

Fit Parameters of Width vs. Frequency		
Filename	Frequency (Relative Error)	Width (Relative Error)
Unknown	122.85 ± 0.26 (0.21%) $[cm]$	39.10 ± 0.90 (2.3%) $[\mu m]$
Unknown E	163.02 ± 0.74 (0.45%) $[cm]$	52.1 ± 1.1 (2.1%) $[\mu m]$
Unknown cpp-c	142.24 ± 0.51 (0.36%) $[cm]$	45.4 ± 1.0 (2.2%) $[\mu m]$

Table II. Calculated unknown sample widths using the calibration between fitted frequency and sample width

3.2. Ethanol Concentration Calibration

The total absorbance amplitude in the range 1000 – $1120 cm^{-1}$ was calculated numerically for each concentration of ethanol in the solution using the trapezoidal rule[12]. Plotting the IR spectrum of all the solutions in that range on the same graph (see Figure 8) shows the increasing intensity of the peaks for higher and higher concentrations of ethanol.

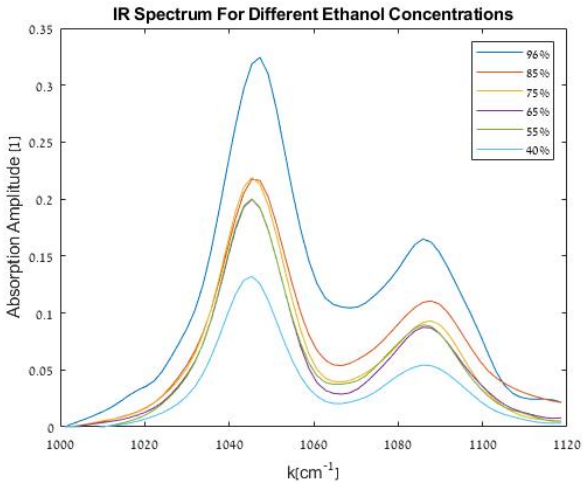

Figure 8. IR spectrum of solutions with different ethanol concentration in the range 1000-1120cm^{-1}

Fitting a linear function according to equation 10 to the measurements of concentration and absorbance yielded the following (see Figure 9).

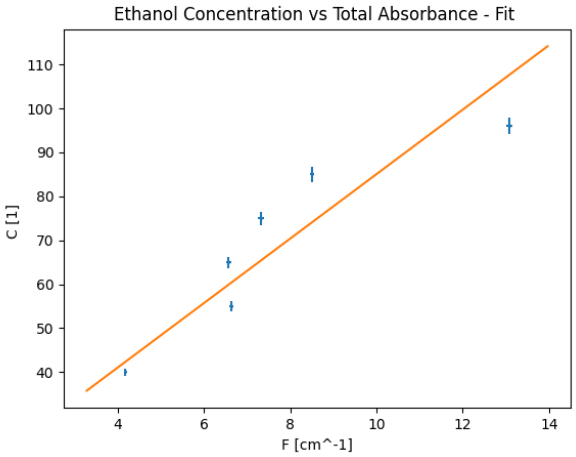

Figure 9. Linear calibration graph of concentration of ethanol in the solution to total absorbance amplitude in the range 1000 – $1120 cm^{-1}$

The fit parameters extracted from the linear fit can be seen in Table III.

Fit Parameters and Statistical Measures of Ethanol Calibration Graph		
Parameter	Value	Error (Relative Error)
$a_0[1]$	11.7	9.3(79%)
$a_1[cm]$	7.3	1.4 (19%)
P_{value}	3.8×10^{-32}	—
χ^2_{red}	38	—

Table III. Fit parameters and statistical measures of the ethanol concentration vs absorption amplitude graph

P_{value} and χ^2_{red} are not in their corresponding desirable ranges, more about that in the discussion. The concentration of ethanol in other solutions was then found by numerically calculating the total absorption in the relevant range and plugging it in the linear equation using the fit parameters. Using the fit parameters from Table III the concentrations in a Suktinis and two unknown alcoholic beverages were found (see Table IV).

Ethanol Concentration in Different Beverages		
Beverage	Concentration(%)	Concentration Error (Relative Error)
Suktinis	54.3	8.3 (15%)
Unknown 1	40.5	5.7 (14%)
Unknown 2	72	12 (17%)

Table IV. Ethanol concentration in different beverages

3.3. CO_2

Using the trapezoidal rule the total absorbance of the air in the region $2270-2400 cm^{-1}$ was calculated. The total absorbance in that region is proportional to the concentration of CO_2 as there are two peaks correlating to CO_2 in said region [11] and in accordance with equation 3, a linear relation is assumed. The ratio between the total absorbance of exhaled air and room air in that region, denoted by S, was calculated. S also represents the ratio between CO_2 as explained above,

$$S = \frac{Absorbance_{Exhaled}}{Absorbance_{Room}} = 61 \pm 24\ (39\%)\ [1] \qquad (14)$$

S would later be compared to that measured a few years ago to see the trend line.

3.4. CO

The absorption peaks from the IR spectrum of CO were extracted and the absorption lines, ΔT, and their corresponding angular momentum transitions, m, were measured relative to the center point at $\Delta T = 2141 cm^{-1}$, ΔT represents $\Delta J = m = 0$ and the vibrational transition from $v = 0$ to $v' = 1$. Using the locations of the absorption peaks, a 3^{rd} order polynomial fit was made according to equation 11 (see Figure 10).

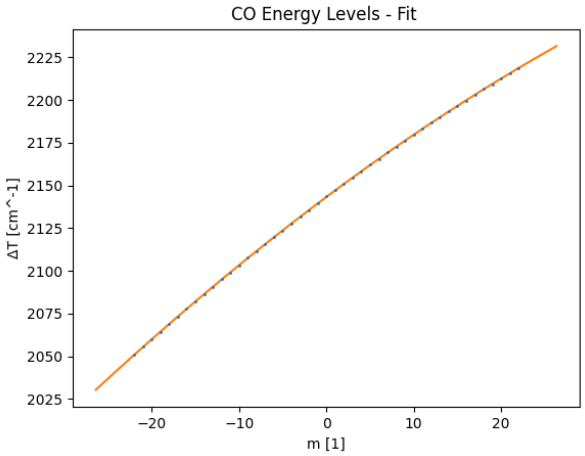

Figure 10. 3^{rd} order polynomial fit of the spectral lines of the absorption peaks ΔT as a function of the transition of CO's angular momentum m.

The fit parameters and statistical measures extracted can be seen at Table V.

Fit Parameters and Statistical Measures of the CO absorption lines 3^{rd} polynomial fit		
Parameter	Value(%)	Error (Relative Error)
$a_0[cm^{-1}]$	2143.293	0.034 (0.0016%)
$a_1[cm^{-1}]$	3.8220	0.0040 (0.10%)
$a_2[cm^{-1}]$	-0.01800	1.5×10^{-4} (0.83%)
$a_3[cm^{-1}]$	-9.4×10^{-6}	1.30×10^{-5} (140%)
P_{value}	0.22	—
χ^2_{red}	1.2	—

Table V. Fit parameters and statistical measures of the 3^{rd} order polynomial fit

Using the fit parameters the coefficients in equation 7 were extracted via the relations stated in equation 12 (see Table VI).

Coefficients of The CO Absorption Lines Equation (equation 7)		
Parameter	Value(%)	Error (Relative Error)
$w_e[cm^{-1}]$	2159.086	0.068 (0.0031%)
x_e [1]	0.007315	1.6×10^{-5} (0.22%)
$B_e[cm^{-1}]$	1.9290	0.0090 (0.47%)
$\alpha\ [cm^{-1}]$	0.01800	1.5×10^{-4} (0.83%)
$D_v\ [cm^{-1}]$	2.4×10^{-6}	3.3×10^{-6} (140%)

Table VI. The coefficients from equation 7 of the CO absorption lines extracted using the fit parameters

3.5. Cigar Smoke's Chemical Makeup Analysis

By looking at the different peak placements and shapes in the IR absorption spectrum of each cigar's smoke and comparing them to the peaks of chemicals with known peaks in the area from the literature[11], the chemical makeup was found. To aid in this endeavor, past research on the subject was consulted (See [13] and [14] in bibliography). The LM00 (as opposed to plain "LM") cigar has the widest range of wave numbers, as such, the LM00 cigar smoke's IR spectrum is shown in Figures 11 and 12. Only "(Brand)'s IR spectrum" is written, to be understood as "The (Brand) cigar smoke's IR spectrum". Other IR spectra are quite similar, Galouis and Canadian have the exact same IR spectrum, down to the noise, thus, only Galouis results are shown. NEXT and Marlboro's IR spectra are only between 2000cm^{-1} and 2400cm^{-1} and LM's is between 2000cm^{-1} and 2520cm^{-1}, therefore, many substances cannot be identified and quantified.

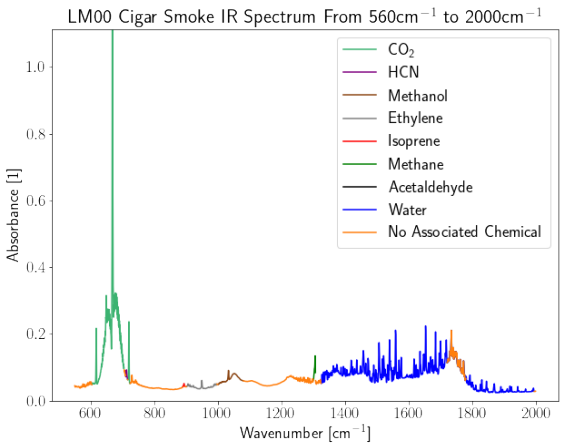

Figure 11. IR Spectrum from 560cm^{-1} to 2000cm^{-1} of LM00 cigar smoke with color-coded regions corresponding to the identifying peaks of each substance.

The region from 400cm^{-1} to 550cm^{-1} was cut from all measurements as it contains much noise and little identifying peaks.

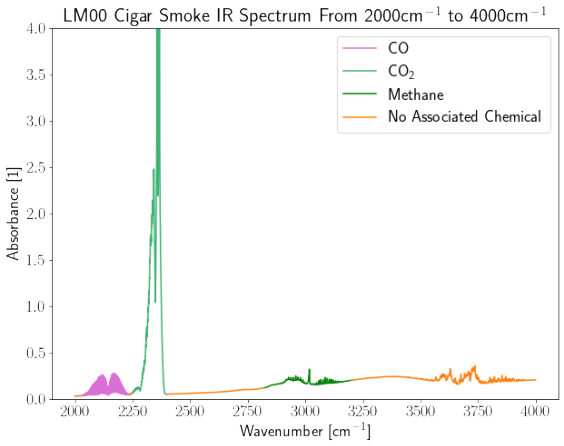

Figure 12. IR Spectrum from 2000cm^{-1} to 4000cm^{-1} of LM00 cigar smoke with color-coded regions corresponding to the identifying peaks of each substance.

Note the bumpy area from 3500cm^{-1} to 4000cm^{-1}, H_2O and CO_2 have been identified in lower wave numbers and this is a mix of the two [14]. The area under each substance region was calculated using trapezoidal rule [12] and is taken as a proxy for substance amount. This metric does not allow for comparison between the substances in a cigar, but does allow for comparison between cigar brands. The identifying regions for each substance and area for each brand are shown in Tables VII and VIII.

Peak Ranges For Substances In Cigar Smoke	
Substance	Range
CO	2028-2238 cm^{-1}
CO_2	604-705 cm^{-1} 717-724 cm^{-1} 2248-2400 cm^{-1}
HCN	710-716 cm^{-1}
Methanol	1000-1080 cm^{-1}
Ethylene	901-997 cm^{-1}
Isoprene	889-897 cm^{-1}
Methane	1300-1307 cm^{-1} 2820-3200 cm^{-1}
Acetaldehyde	1720-1780 cm^{-1}
H_2O	1325-1994 cm^{-1}

Table VII. Identifying regions for the found substances.

Area Under Identifying Regions For Each Cigar Brand					
Substance	NEXT	Marlboro	LM	Galouis	LM00
CO	18	6.6	12	18	22
CO_2	180	69	140	170	240
HCN	-	-	-	0.37	0.51
Methanol	-	-	-	4.5	4.3
Ethylene	-	-	-	3.1	3.2
Isoprene	-	-	-	0.28	0.35
Methane	-	-	-	64	91
H_2O	-	-	-	43	51
Acetaldehyde	-	-	-	-	-
Acrolein	-	-	-	-	-
Acetone	-	-	-	-	-

Table VIII. Area under the identifying regions of each substance in each brand's smoke.

Every substance was identified based upon its characteristic absorption lines[11][13]. Some regions contain multiple absorption lines that overlap, thus restricting the ability to identify the substances that make them up, such as the region of 1300 – 2000cm^{-1} that contains water's peaks but also many other substances such as acetone, acetaldehyde and acrolein [14], which is why acetaldehyde's total absorption could not be estimated. NEXT and Marlboro's IR spectra are cut short, only CO and CO_2 absorption lines were identified (see Figure 13). As CO and CO_2 are present in all smoke spectra a comparison between the different brands is possible. Note that CO_2 has absorption lines outside the region 2000 – 2400cm^{-1} and thus outside NEXT and Marlboro's IR spectra. As such, the only valid comparison is in the 2000 – 2400cm^{-1} region. The ratios of total absorbance between cigars, which according to equation 3 is also the ratio between concentrations, was calculated.

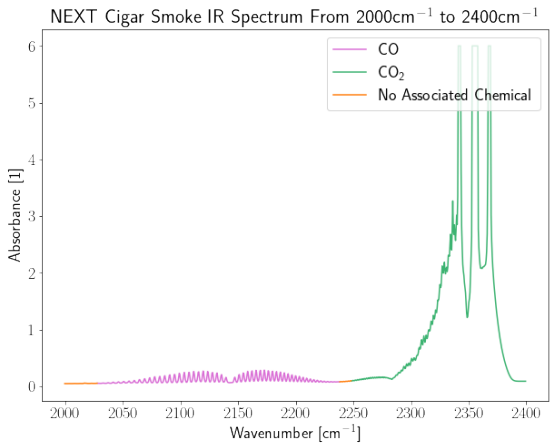

Figure 13. IR Spectrum from 2000cm^{-1} to 2400cm^{-1} of NEXT cigar smoke with color-coded regions corresponding to the identifying peaks of each substance.

Calculating the ratios between the total absorbance of CO_2 in the region 2248-2400 cm^{-1} and CO in the region 2028-2238 cm^{-1} yielded the following ratios (see Table IX and Table X). The ratios of CO_2 were calculated using outside air as a baseline, whose CO_2 total absorption in that region was previously measured. Using the concentration of CO_2 in air, $C_{CO_2} = 0.041\%$ [15], the concentration of CO_2 in the smoke from the cigars was found as well.

Ratios of CO_2 For Different Cigars With Outside Air As A Baseline					
Property	NEXT	Marlboro	Galouis	LM00	LM
CO_2 Ratio	120	44	140	100	83
CO_2 Concentration	4.9%	1.8%	5.7%	4.1%	3.4%

Table IX. Ratios of CO_2 for different cigars with room air as a baseline.

The ratios of CO were calculated using the NEXT cigar as the baseline (see Table X) since no measurement of CO's IR spectrum in air was made in this experiment.

Ratios of CO for Different Cigars			
Marlboro	Galouis	LM00	LM
0.36	1	1.2	0.82

Table X. Ratios of CO for different cigars with NEXT cigar as a baseline.

The remaining ratios of gases can only be calculated between the Galouis and LM00 cigars since the other two cigars contain only CO and CO_2 absorption lines in their spectrum. These remaining ratios would be referred two in the discussion and can be also calculated directly from Table VIII.

4. DISCUSSION

4.1. Thin Polyester Film

The refractive index of the polyester was found, and the relationship between the sample width and destructive interference frequency was calibrated. The frequency of each sample was extracted by fitting a sine wave to the area with the clearest sine. For thin (compared to other samples) widths, the region of 2200 – 2600 cm^{-1} has particularly clear sine waves. Other regions of interest are 550 – 800 cm^{-1} and 3200 – 3320 cm^{-1} which are used when clear enough and the aforementioned region is of little use. All sine fits are very good apart from that of 24 μm, whose IR spectrum did not contain a sine but still had a periodicity in the 2200 – 2600 cm^{-1} region. The linear fit between width and frequency is clear, with all points within less than two standard deviations away from the line. The slope's standard deviation is within accepted levels, and the intercept is less than two standard deviations from its theoretical value. The extracted widths are interpolated using the calibration. The widths are inline with measured widths. The extracted refractive index is in the general area of plastics' refractive indices [16]. As this is an average over the range of wave lengths in the interferogram, pinpointing which plastic in particular is used is impossible from the refractive index alone. Using the IR spectrum to further narrow down options may be possible, but is out of the scope of this report.

4.2. Ethanol

In this part of the experiment we measured the IR spectrum of solutions with different yet known ethanol concentrations and calculated the total absorption amplitude of the solutions in the range $1000 - 1120 cm^{-1}$ where there are absorption peaks of ethanol. A calibration graph between the concentration of ethanol in the solution and the total absorption amplitude in that range was made using a linear fit according to Beer-Lambert Law from equation 3. Using the calibration graph, the concentration of ethanol in different beverages was found. The concentration for Suktinis, $C_{Suktinis} = 54.3 \pm 8.3$ ($R.E\ of$ 15%) came out close to the written value of 50% with $N\sigma = 0.52$ [17] which confirms the validity of our calibration to a certain degree. However, as can be seen in figure 9 as well as in table III, the linear fit does not represent the data accurately and that a fit to a polynomial of a 2^{nd} degree or higher could have yielded better results. Possible reasons for the somewhat inadequate fit can be that equation 3 only holds for low concentrations, whereas the concentrations in this experiment went as high as 96%. In addition to that, the absorption peaks of ethanol have some width, and the total absorption is calculated for a number of wavelengths in that range, whereas the coefficient in the Beer-Lambert Law is wavelength dependent and not constant for the entire range. The consequences of

the latter effect can also be seen in figure 8 where the absorption amplitude changes differently depending on the wavenumbers. Regardless, the linear fit did sufficiently well and yielded good results.

4.3. CO_2

The ratio between the CO_2 content of alveolar air (exhaled air) and fresh indoor air (inhaled air) was calculated to be $S_{2020} = 61$. This ratio was also calculated for 1998 to be $S_{1998} = 72.2 \pm 1.4$ with the percentage of CO_2 in alveolar air taken to be 5.3%[18], indoor CO_2 levels had to be approximated conservatively as twice the CO_2 content measured outside, at 730 ppm[19], this conservative approximation lowers S_{1998} further. Noting both approximations, a downward trend is seen, were this trend to continue indoor and later outdoor CO_2 levels will become too high for comfort or life in the nearing decades (for a more in depth analysis see [20]).

4.4. CO

The IR spectrum of CO was measured in the range 2025 – 2233cm^{-1} where there are absorption lines correlating to the angular momentum and vibrational transitions of the diatomic molecule. The resulting IR spectrum came out similarly to that described in the literature [21]. There are two symmetrical absorption regions around a center point at 2141cm^{-1} with nearly no absorption compared to its surroundings. Using the IR spectrum's absorbance peaks, a 3^{rd} order polynomial fit was made according to equation 7 with $v' = 1$ as this is the relevant transition in the region measured. The fit validated the theory as can be seen in figure 10. This claim is also supported by the statistical measures (see Table V) which are within their appropriate regions. Using the fit parameters, the coefficients in equation 7 were calculated using the relations in equation 12. The coefficients were then compared with their corresponding theoretical values from the literature [21] (see Table XI)

Comparison with Theoretical Values of the Coefficients In Equation 7			
Coefficient	Theoretical Value	$N\sigma$	Relative Distance
$D_v[cm^{-1}]$	6.2×10^{-6}	1.2	61%
$B_e[cm^{-1}]$	193.13×10^{-2}	3.2	1.5%
$\alpha[cm^{-1}]$	1.75×10^{-2}	3.3	5.0%
$w_e[cm^{-1}]]$	2169.8	160	0.51%
$w_e x_e[cm^{-1}]$	13.29	72	19%

Table XI. Comparison of the calculated coefficients with their corresponding theoretical values taken from the literature [21]

The relative distances were calculated in addition to the calculation of $N\sigma$ as in some cases the relative error of the calculated coefficients was either too small or too big, therefore $N\sigma$ was not indicative of the closeness between the two compared values. Overall the calculated coefficients came out close to the corresponding theoretical ones, with those who are somewhat far sharing the same scale with them. In conclusion, the results are satisfactory and indicate the validity of our model and measurements.

4.5. IR Spectrum Analysis of The Smoke From Many Cigar Brands

Many substances were identified, with the aide of past publications, in the IR spectra of the smokes. As some brands' IR spectra only include a limited wave length region, not all substances were identified and quantified in each brand's smoke. Noting that fact, a comparison between the cigars and the health risks that come with each is made. As most substances were not identified in the brands lacking a wide IR spectrum, a full comparison cannot be made. The comparison is by no means a buyer's guide, as will soon be apparent, cigar smoking is dangerous to life and to be avoided.

The harmful effects of each of the identified substances will now be listed. These effects may not necessarily occur for the concentrations in a cigar. As the concentrations were not measured, this report will be based on previous literature on the toxicity of cigars and cigarettes.

Starting from the top of Table VIII, carbon-monoxide (CO) can take the place of oxygen in blood transport and negatively affect the heart [22] and dexterity.

As stated in PubChem[23]: "The first symptoms of carbon monoxide exposure when carboxyhemoglobin (COHb, carbon monoxide taking the place of oxygen in the blood) is 15-30% are generalized, and may include: headache, dizziness, nausea, fatigue, and impaired manual dexterity. Individuals with ischemic heart disease may suffer from chest pain and decreased exercise duration at COHb levels measured from 1% - 9%". Cigar smokers have COHb levels ranging from 13% to 39% and are reported to experience the above symptoms [24].

Next up is CO_2. As should be obvious, CO_2 poisoning can happen, however, no report stating that CO_2 poisoning is a risk in cigar smoking under normal circumstances was found.

After CO_2, comes hydrogen cyanide (HCN). HCN can negatively affect the central nervous system, thyroids, lungs and heart [22][25].

With a villainous effect on smokers comes methanol. Methanol is added to cigars and cigarettes to "mask unpleasant flavors and harshness of tobacco products, making them easier to start using. Tobacco products with menthol can also be more addictive and harder to quit by enhancing the effects of nicotine" [26]. This flavour also adds to the appeal of tobacco to young adults and teens [26].

Now onto ethylene. As with CO_2, no literature was found that states ethylene is potentially dangerous in cigars.
Continuing to isoprene. Isoprene is a possible carcinogen and may be a central nervous system depressant [27].
Below isoprene sits methane. As with ethylene, no literature was found which warns of the methane content of cigars and cigarettes.
H_2O is next up for examination. No literature suggests H_2O is of much danger in cigars.
Now onto the last three substances, acetaldehyde, acrolein and acetone. While a comparison is not possible, it is of importance to mention their effects. Acetaldehyde is a group 1 carcinogen (meaning it is highly likely to cause cancer) and is the most abundant carcinogen in cigar smoke [28][29], it also causes "nasal olfactory epithelial lesions" [22]. It is water-soluble, as such, it remains in the smoker's saliva which furthers the exposure. Its origin is partly in the combustion of added sugars that mask the cigar's taste. It has also been shown that acetaldehyde enhances nicotine absorption in rats [30], since then, cigarette companies have looked for the optimal ratio of acetaldehyde and nicotine, "based on the results of internal research, Philip Morris increased the level of acetaldehyde in Marlboro cigarettes by 40% between 1982 and 1992 through the addition of sugars [31]" as stated in [32].
Acrolein in cigar smoke may cause nasal lesions [22], and acetone may cause neurological effects [22].

Looking at VIII and using our newly formed substance toxicity expertise, "LM00" is the worst cigar health-wise as it has the highest CO content, the highest HCN content, is it a close second in methanol and a first in isoprene.

[1] M. R. Derrick , D. Stulik and J. M. Landry, *Infrared Spectroscopy in Conservation Science* (The Getty Conservation Institute, 1999).

[2] H. N. Hsieh, *Ftir instrumentation* (2008), URL https://studentportalen.uu.se/uusp-filearea-tool/download.action?nodeId=111007&toolAttachmentId=44350.

[3] *Fundamentals of Photonics* (John Wiley and Sons, Ltd, 1991), ISBN 9780471213741, https://onlinelibrary.wiley.com/doi/pdf/10.1002/0471213748, URL https://onlinelibrary.wiley.com/doi/abs/10.1002/0471213748.

[4] LibreTexts, *Beer's law*, https://chem.libretexts.org/Courses/Providence_College/CHM_331_Advanced_Analytical_Chemistry_1/08\%3A_An_Introduction_to_Ultraviolet-Visible_Absorption_Spectrometry/8.02\%3A_Beer\'s_Law.

[5] N. L. Alpert , W. E. Keiser and H. A. Szymanski, *IR Theory and Practice of Infrared Spectroscopy* (Plenum Press New York, 1970).

[6] D. J. Griffiths, *Introduction To Quantum Mechanics* (Pearson Education International, 2005).

[7] J. Sakurai and J. Napolitano, *Modern Quantum Mechanics Second Edition* (Pearson Education International, 2011).

[8] B. H. Stuart, *Infrared Spectroscopy: Fundamentals and Applications* (John Wiley and Sons, Ltd, 2004).

[9] *Introduction to Fourier Transform Infrared Spectroscopy*, Thermo Fisher Scientific Inc (2013).

[10] Attenuated total reflectance, *Attenuated total reflectance — Wikipedia, the free encyclopedia* (2013), [Online; accessed 15-December-2021], URL https://commons.wikimedia.org/wiki/File:ATR_path-en.svg.

[11] National Institute of Standards and Technology, U.S Department of Commerce, *Nist chemistry webbook, srd 69* (2021), URL https://webbook.nist.gov/chemistry/name-ser/.

[12] W. H. Press, S. A. Teukolsky, W. T. Vetterling and B. P. Flannery, *Numerical Recipes The Art of Scientific Computing Third Edition* (Cambridge University Press, 2007).

[13] N. Garizi, A. Macias, T. Furch, R. Fan, P. Wagenknecht and K. A. Singmaster, Journal of Chemical Education **78** (2001), URL http://www.columbia.edu/itc/chemistry/c2507/CS_Material_04/CS2_Material_2.pdf.

[14] A. R. Ford , W. A. Burns and S. W. Reeve, Journal of Chemical Education **81** (2004).

[15] B. Auis, *The atmosphere: Getting a handle on carbon dioxide* (2019), URL https://climate.nasa.gov/news/2915/the-atmosphere-getting-a-handle-on-carbon-dioxide/.

[16] N. Sultanova, S. Kasarova and I. Nikolov, *Dispersion Properties of Optical Polymers* (Proceedings of the International School and Conference on Photonics, 2009).

[17] *Suktinis mead 1l*, [Online; accessed 21-December-2021], URL https://www.theliquorbarn.com/suktinis-mead-1l.

[18] R. S. Carel, *Handbook of Air Pollution from Internal Combustion Engines Pollutant Formation and Control* (Academic Press, 1998), chap. 3, p. 74.

[19] P. Tans and R. Keeling, ESRL (www.esrl.noaa.gov/gmd/ccgg/trends/) (2009).

[20] T. A. Jacobson, J. S. Kler, M. T. Hernke, R. K. Braun, K. C. Meyer, and W. E. Funk, Nature Sustainability **2**, 691 (2019), ISSN 2398-9629, URL https://doi.org/10.1038/s41893-019-0323-1.

[21] N. Mina-Camilde, C. Manazanares I, J. F. Caballero, Journal of Chemical Education **73** (1996).

[22] Talhout R, Schulz T, Florek E, van Benthem J, Wester P and Opperhuizen A., International journal of environmental research and public health **8** (2011).

[23] N. C. for Biotechnology Information, *PubChem Compound Summary for CID 281, Carbon monoxide.*, Retrieved December 21, 2021 from https://pubchem.ncbi.nlm.nih.gov/compound/Carbon-monoxide. (2004).

[24] A. Dorey, P. Scheerlinck, H. Nguyen, BG T. Albertson, MILITARY MEDICINE **185** (2020).

[25] N. C. for Biotechnology Information, *PubChem Compound Summary for CID 768, Hydrogen cyanide.*, Retrieved December 21, 2021 from https://pubchem.ncbi.nlm.nih.gov/compound/Hydrogen-cyanide. (2004).

[26] U. Food and D. Administration, *Fda commits to evidence-based actions aimed at saving lives and preventing future generations of smokers*, FDA News Release (2021).

[27] N. C. for Biotechnology Information, *PubChem Compound Summary for CID 6557, Isoprene.*, Retrieved December 21, 2021 from https://pubchem.ncbi.nlm.nih.gov/compound/Isoprene. (2004).

[28] The International Agency for Research on Cancer (IARC), *Re-*

evaluation of Some Organic Chemicals: Hydrazine and Hydrogen Peroxide (Part Two) (IARC Monographs on the Evaluation of the Carcinogenic Risks to Humans, 71) (World Health Organization, 1999).

[29] M. Salaspuro, Scandinavian Journal of Gastroenterology **44**, 912 (2009), https://doi.org/10.1080/00365520902912563, URL https://doi.org/10.1080/00365520902912563.

[30] J. D. Belluzzi, R. Wang, and F. M. Leslie, Neuropsychopharmacology **30**, 705 (2005).

[31] C. Bates and M. Jarvis (1999).

[32] G. F. Wayne, G. N. Connolly, and J. E. Henningfield, Nicotine and Tobacco Research **6**, 927 (2004), ISSN 14622203, 1469994X, URL http://www.jstor.org/stable/26760248.